Advance Journal of Food Science and Technology 8(6): 383-393, 2015
DOI:10.19026/ajfst.8.1531
ISSN: 2042-4868; e-ISSN: 2042-4876

Submitted: November 13, 2014 Accepted: January 8, 2015 Published: June 10, 2015

Research Article

Modeling the Mechanical Texture of Foxtail Millet Extrudates during Hydrosorption with a Modified Peleg-Fermi Model

[1]Xuewei Zhao, [1]Guangjie An, [1]Zhangcun Wang and [2]Yimin Wei
[1]School of Food and Bioengineering, Zhengzhou University of Light Industry, Zhengzhou 450002, China
[2]Institute of Agro-food Science and Technology, Chinese Academy of Agricultural Sciences, Beijing 100193, China

Abstract: The objective of this study was to monitor and model the texture changes of foxtail millet extrudates with different structural properties as a function of water activity (a_w). Four extrudates, after equilibrated at a_w of 0.113-0.97, were compressed using a TA.XT2 Texture Analyzer. Two force-related texture parameters, Peak Force (PF) and Total Work (TW) and two jaggedness-related, Number of Spatial Ruptures (NSR) and Specific Ling Length (SLL), were extracted from their force-displacement curves. Water sorption led to loss of jaggedness of their force-displacement curves. All the four texture parameters decreased when a_w increased to a certain value. Before the decrease occurring, *TW* and *PF* increased for all the extrudates with a_w increase, while *SLL* increase was observed only for two extrudates and no *NSR* increase was observed for all extrudates. The critical water activity (a_{wc}) where texture parameters decreased rapidly ranged between 0.42 and 0.83 depending mainly on the kinds of the extrudates and to some extent on the texture parameters studied. The extrudates with coarse structure exhibited lower force-related values, while the extrudates with fine structure exhibited lower jaggedness-related values. Crispness index, a combination of force- and jaggedness-related texture criteria, decreased almost linearly as a_w increase up to 0.61~0.66 for all the extrudtes. The Peleg-Fermi equation can satisfactorily model the changes in jaggedness-related texture parameters as a function of a_w. A modified form of the Peleg-Fermi equation, proposed in this study, was needed to model the changes of force-related parameters better.

Keywords: Extrusion, foxtail millet, hydrosorption, modeling, Peleg-Fermi model, texture

INTRODUCTION

Most low moisture cellular foods such as extruded cereals have a crispy texture, which is determinant to their behavior in consumption. Sensory and instrumental measurement (including acoustic and mechanical testing) of crispness has been extensively studied (Katz and Labuza, 1981; Heidenreich *et al*., 2004; Saeleaw *et al*., 2012). There is particular interest in the latter since instrumental methods overpass the deficiencies in sensory tests by short time, lower cost and better reproducibility and are independent of the psycho-physiological condition of panelists (Surówka, 2002). Many researches have been conducted in afford to explore the relationship between crispness intensity and instrumental texture parameters (Saeleaw *et al*., 2012; Chauvin *et al*., 2008).

Of course, the texture of extruded products is dependent mainly on their processing parameters and raw material compositions. Once an extrudate is produced, post-extrusion changes will take impacts on its texture. Water and temperature are, by far, the most investigated factors due to their relevance in affecting their quality and stability. Dry cereal extrudates are hygroscopic due to chemical composition, porosity and presence of starch in amorphous state (Colonna *et al*., 1984). If the moisture of these products increases, due to water sorption from the atmosphere, it results in a soggy, soft texture (Nicholls *et al*., 1995) and loses its crispness. Then, the effects of hydrosorption on texture are well documented on cereal extrudates (Barret and Kaletunc, 1998; Pamies *et al*., 2000; George *et al*., 1989; Heidenreich *et al*., 2004).

Modeling the volution of texture properties during water sorption helps to predict the crispness and select proper storage conditions. Peleg-Fermi equation was widely used in literatures to model the texture changes with a_w increase (Pamies *et al*., 2000; Harris and Peleg, 1996; Suwonsichon and Peleg, 1998; Braga and Cunhn, 2004). Peleg-Fermi equation assumes that a linear relationship exists between a texture property and moisture activity before the decrease of the property. However, Gondek and Lewicki (2006) found that the relationship between both force and work of compression and water activity in corn flakes could not be described by the Peleg-Fermi equation. The

Corresponding Author: Xuewei Zhao, School of Food and Bioengineering, Zhengzhou University of Light Industry, Zhengzhou 450002, China, Tel./Fax: +86-371-8860-9631

relationship was curvilinear, bend downwards and the slope increased with increasing water activity until water activity reached critical value. Such a evolution with a_w was also observed for compression force of extruded flat rye bread (Marzec and Lewicki, 2006), bend work of corn-rye bread (Lewicki *et al*., 2004), hardness for extruded waxy maize (Roudaut and Champion, 2011), mean and maximum force of rice crisp (Heidenreich *et al*., 2004), even for flexural and compressive fracture strain of dried bread (Chang *et al*., 2000), penetration depth for corn flakes (Sauvageot and Blond, 1991).

The primary objective of this work was to test the variation of different mechanical texture parameters of foxtail millet extrudates with different physical properties as a_w increase and modify the Peleg-Fermi equation if necessary to model the texture evolution with a_w.

MATERIALS AND METHODS

Extrudate samples: The composition of the foxtail millet grain was 10.40% protein, 1.96% lipids, 1% fiber and 86.64% carbohydrate (by difference). Foxtail millet extrudates were produced using a pilot-scale, co-rotating, intermeshing, twin-screw extruder typed DSE-25 (Brabender GmbH and Co., Germany) from a center-composite experimental design. All the products were divided into four classes according to their morphology (Zhao, 2006). Four samples were selected with each from one category. Their physical properties are showed in Table 1. The 1# sample showed a coarsest structure characterized by least numerous and largest mean size of air cells with thickest wall. The 4# sample had most numerous and smallest air cell with thinnest wall and narrowest distribution in cell size. The other two samples had structural properties between the two limits, with 2# sample more close to 1# sample and 3# sample to 4# sample.

Sample equilibration: The four samples were dried, cut to 20-cm lengths and placed in evacuated desiccators over saturated solutions of LiCl, CH_3COOK, $MgCl_2$, K_2CO_3, Mg $(NO_3)_2$, NaBr, $NaNO_2$, NaCl, KCl and K_2SO_4 at an ambient temperature of 25°C for 4 weeks. This corresponds to a_w levels of 0.11, 0.23, 0.33, 0.43, 0.52, 0.57, 0.65, 0.75, 0.85 and 0.97, respectively (Greenspan, 1977). Thymol was used to prevent microbial growth at the high a_w levels. Following equilibration, the samples were subjected to mechanical texture analysis.

The moisture contents were measured in triplicate by drying weighed samples of the product in an oven at 105°C for 3 h (Lane, 1998).

Acquisition of mechanical data: The equilibrated extrudates were cut to 20 mm long specimens with a sharp blade, then compressed using a TA-XT2 texture analyzer (Stable Microsystems, Godalming UK) fitted with a 50-mm diameter cylindrical flat-faced probe. The speeds of pre-test, test and post-test were 1, 0.5 and 1 mm/sec, respectively. Data were acquired with a resolution of 200 Hz. All samples were compressed to 60% deformation and 15 measurements were carried out for each sample. From the force-deformation data the following parameters were derived.

Peak force (PF, N): The maximum force during compression deformation.

Total work (TW, N·m): The area under the force-distance curve.

Number of spatial ruptures (NSR, mm^{-1}): The ratio of the total number of force peaks to deformation distance.

Specific line length (SLL, -): The ratio of line length of the force-deformation curve to the deformation distance. The line length was calculated using the Pythagoras's equation (Norton *et al*., 1998):

$$LL = \sum_{i=0}^{n} \sqrt{\Delta F^2 + \Delta L^2} \quad (1)$$

Crispness index (CI, -): The ratio of *SLL* to the product of *TW* and *PF*.

An average value of each parameter was calculated on the basis of 15 replicates tested at each moisture level.

Modeling the texture properties: The relationship between textural parameters and a_w can assume various shapes as shown in Fig. 1. The most frequently encountered type has a characteristic sigmoid shape that can be described by the Fermi distribution function (Wollny and Peleg, 1994):

$$Y = \frac{Y_0}{1 + \exp\left(\frac{a_w - a_{wc}}{b}\right)} \quad (2)$$

where, Y (a_w) is the magnitude of the mechanical parameter, Y_0 is its magnitude in the dry state, a_{wc} is a

Table 1: longitudinal section, diameter and bulk density of the four extrudates used in this study

Samples	1#	2#	3#	4#
Longitudinal Section				
Averaged dia.(mm)	15.89	11.17	9.76	6.77
Bulk density (cm^3/g)	4.73	3.29	4.02	5.57

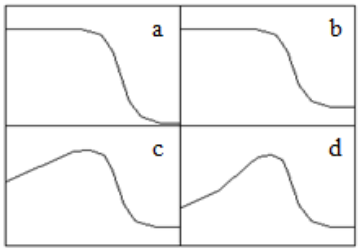

Fig. 1: Schematic view of different possible relationships between a texture property and water activity

characteristic a_w where, Y (a_{wc}) = $Y/2$ and b is a constant accounting for the steepness of the relationships around a_{wc}. This model fits a graph shown in Fig. 1a.

In some cases, the wet material still retains a considerable level of texture magnitude as described in Fig. 1b. The Fermi model was modified by adding a term which account for residual magnitude (Y_r) and assumes the form of Eq. (3) (Wollny and Peleg, 1994):

$$Y = \frac{Y_0 - Y_r}{1 + \exp\left(\frac{a_w - a_{wc}}{b}\right)} + Y_r \quad (3)$$

Equation (2) and (3) assume that Y is constant at low to intermediate a_w levels. When a maximum of texture properties has appeared (Fig. 1c) with a_w increase, the evolution pattern could be described using a modified form of the Eq. (2) called Peleg-Fermi model (P-F model) (Harris and Peleg, 1996) through adding a linear term of ka_w to Y_0 in Eq. (2):

$$Y = \frac{Y_0 + ka_w - Y_r}{1 + \exp\left(\frac{a_w - a_{wc}}{b}\right)} + Y_r \quad (4)$$

where, k is a constant, roughly the slope of the linear region.

In some cases, Y would increase with a_w following a power relation before decrease (Fig. 1d). Then, we modified Eq. (4) further by replacing the linear term ka_w with ka_w^n Eq. (5) and called it modified Peleg-Fermi model (MP-F model) in the following text:

$$Y = \frac{Y_0 - Y_r + ka_w^n}{1 + \exp\left(\frac{a_w - a_{wc}}{b}\right)} + Y_r \quad (5)$$

Regression and statistical analysis: In order to evaluate the goodness of fit between the experimental and predicted, data a statistics package STATISTIC for Windows (Version 6.0) was used to conduct non-linear regression process. The following three error parameters are used for comparison.

Residual Sum-of-Squares (RSS) is defined as follows:

$$RSS = \sum_{i=1}^{m} (V - \bar{V})^2 \quad (6)$$

where,
m = The number of data points
$V, \bar{V}$ = Observed and averaged values of independent variable

The Standard Error of Estimate (SEE) shows the deviation of the dependent variable and is given by:

$$SEE = \sqrt{\frac{\sum_{i=1}^{m} (V - \bar{V})^2}{d_f}} \quad (7)$$

where, d_f is degree of freedom.

The Mean Relative Deviation (MRD) gives an idea of the mean departure of the measured data from the predicted data. It is expressed as:

$$MRD = \frac{1}{m} \sum_{i=1}^{m} \frac{|V - \bar{V}|}{V} \quad (8)$$

In these error parameters, the *RSS* value is an important parameter in the non-linear regression process. The *SEE* value represents the fitting ability of a model in relation to the number of data points. The fitted equation giving the smallest *SEE* value for the same set of experimental data yields the best results. However, the *SEE* value cannot provide a direct visualization of the goodness-of-fit. For this reason, the *MRD* is used to describe the goodness-of-fit of an equation. Therefore, the smaller the *MRD* value, the better the goodness-of-fit.

RESULTS AND DISCUSSION

Water sorption isotherms: Figure 2 presents isotherms of water vapor sorption for the four extrudates. The isotherm curves are sigmoid in shape and typical for cereal-based products. As a_w increased from 0.11 to 0.75, equilibrium moisture content increased only gradually. At higher a_w, the increase became sharp. The values of equilibrium moisture contents of each sample were very close at same a_w level, although the four extrudates had very different structural properties.

Katz and Labuza (1981) reported that at moisture content larger than the Brunauer-Emmett-Teller (BET) monolayer the consumer perceives a textural change of snack food products. Martinez-Navarrete *et al*. (2004) observed a plasticizing effect of water on wafers above the monolayer water content. To determine the monolayer moisture content, the Guggenheim-Anderson-de Boer (GAB) sorption model Eq. (9), one of the most reliable ones for sorption isotherms, was fitted to all the water sorption data of the four samples:

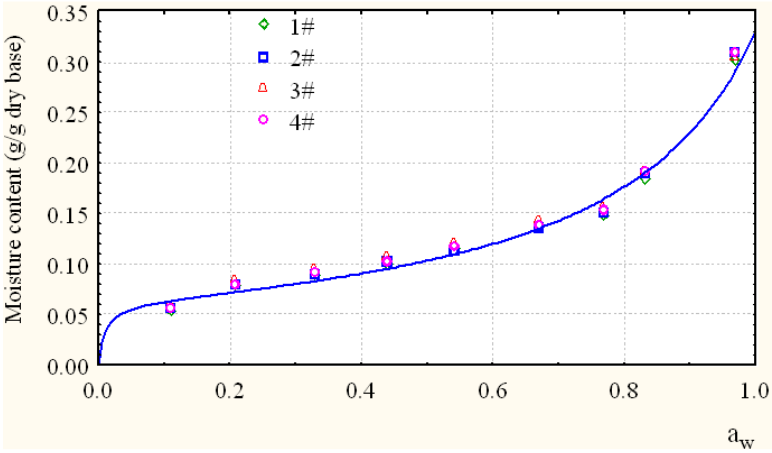

Fig. 2: Equilibrium water content vs. a_w plot for the four foxtail millet extrudates (symbols) and the average GAB sorption isotherm (solid line)

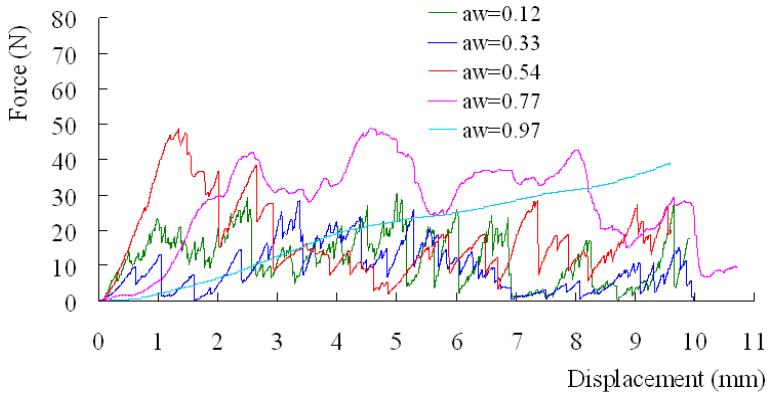

Fig. 3: Force-displacement curves of 1# extrudate equilibrated at a_w 0.12, 0.33, 0.54, 0.77 and 0.97, respectively

$$M_e = \frac{M_m K C a_w}{(1 - K a_w)(1 - K a_w + C K a_w)} \quad (9)$$

where,

M_e = The moisture content after water sorption equilibrium

M_m = A constant representing the moisture content adsorbed as a monomolecular layer

C, K = Constants related to the interaction between the first layer and further layers of water molecules at the sorption sites

Good fit was observed with R^2 = 0.9904. The monolayer moisture contents determined by the GAB equation was 0.0621 g/g, corresponding to a_w 0.097. Values of the GAB constants, C and K, were 167.9745 and 0.8195, respectively. The result was lower than the monolayer moisture of the white corn cake 5.11% (Li *et al*., 1998), but very close to that of wafers 6.2% (Martinez-Navarrete *et al*., 2004).

Effects of hydrosorption on force responses during compression: Examples of typical force-displacement curves of 1# sample after water sorption equilibrium are presented in Fig. 3. For clarity, only five curves at a_w levels of 0.12, 0.33, 0.54, 0.77 and 0.97, respectively have been selected for the figure. When water activities were lower than 0.54, the force-time relationship is jagged and very irregular, which was typical for a crispy (or brittle) product (Wollny and Peleg, 1994). There seems to be two kinds of force peak: main peak and secondary peak. One main peak can be composted of several secondary peaks. Each peak represented that a fracture event had occurred. The main peak was the result of fracture events occurring in succession. The valley values were almost close to zero especially at lager deformation for samples conditioned at lower a_w. The jaggedness degree decreased with the increase in water activity. The magnitude of the force drops at the major fracture point also increased. Similar observation has been reported for extruded cereals (Heidenreich *et al*., 2004; Nicholls *et al*., 1995). When water activity reaches to 0.77, a relatively smoothed curve was observed and the force remained at a considerable high level. For the sample equilibrated to a_w 0.97, only a very smooth curve was obtained indicating no breaking event had occurred.

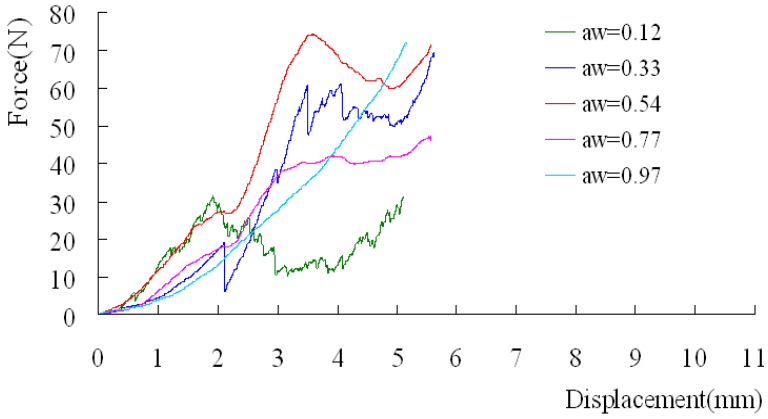

Fig. 4: Force-displacement curves of 4# extrudate equilibrated at a_w 0.12, 0.33, 054, 0.77 and 0.97, respectively

The jagged pattern of the force-displacement curves reflects the fracture behavior of the extrudates. The very irregular and irreproducible force-deformation relationships at lower a_w seems due to the non-uniformity in internal structure (Table 1) and the multiple fracture events during compression of the cellular extrudates. Loss of jaggedness with a_w increase indicated the change in mechanics of compression from rapid unstable brittle fracture at low water content to plastic fracture at higher water activities and finally to elastic deformation.

The force-displacement curves of 4# sample equilibrated at the five a_w levels are presented in Fig. 4. For convenience of comparison, identical axis scaling was taken in Fig. 3 and 4. The force-deformation curves of 4# were different in many respects from those of 1# sample. The 4# extrudate had less force peak and smaller drop-off during compression. The force increase with a_w before breaking was also more gradual for 4# sample. Additionally, at a_w 0.54, the force curve of 4# sample had already become smoothed, while the curve of 1# sample still remained very jagged. Probably, it is because that the pores in 4# sample are significantly smaller than that in 1# sample (Table 1). No distinct breaking peak was observed at the early stages of the test for 4# sample equilibrated at a_w 0.54 and 0.77 and only a yield point appeared. As a whole, the force levels of 4# samples were higher than that of the 1# sample.

The Gibson-Ashby model divided a typical force-deformation curve for brittle foams under compression into three distinct regions (Gibson and Ashby, 1988). The first is a linear elastic compression at smaller deformation, characterized by a straight rise in force with deformation. The second region appears after first breaking, is characterized by several rapid ups and downs in the curve but showing a marginal increase trend for brittle fracture and by a relatively flattened curve for plastic fracture. At the final stage, force continues to increase with increasing deformation due to compaction or densification of the material. The deformation process of 4# sample under compression followed loosely the Gibson and Ashby model, which was proposed for cellular foams with uniform and fine air cells. While for 1# extrudate, its curves composed of only the former two regions and third regions was not observed under the deformation degree applied in this study.

Modeling TW and PF: *PF* and *TW* of the 4 samples plotted against water activity are presented on Fig. 5 and 6, respectively. Generally, lowest *PF* and *TW* values were registered for 1# sample and the higher values were for 3# and 4# samples. At a_w lower than 0.33, difference magnitudes of both *PF* and *TW* among the four extrudates were limited and reach a maximum at about a_w 0.6-0.7, then decreased with further increase of a_w. The 1# sample had the largest diameter, then experienced longest distance of compression. Considering that the *TW* is the area below the force-displacement curve, the mean force during compression of the 1# sample should be much lower than the other three extrudates. It is hypothesized that larger cell size had make its cell wall (behaves as a beam during deformation) easy to break under compression. Previous report showed that the presence of some large cells would clearly decrease both the modulus and fracture stress of sponge structures (Guo and Gibson, 1999).

As shown in Fig. 5 and 6, the variation of *PF* and *TW* of the four extrudates upon moisture sorption followed a similar direction but not an identical pattern. All the texture parameters increased slightly when water activity was less than about 0.33, then increased more rapidly on increasing the a_w up to about 0.6~0.75 depending the kind of extrudates, indicating a hardening effect of hydration. With both *WT* and *PF*, their increase was greater for samples 3# and 4#. The

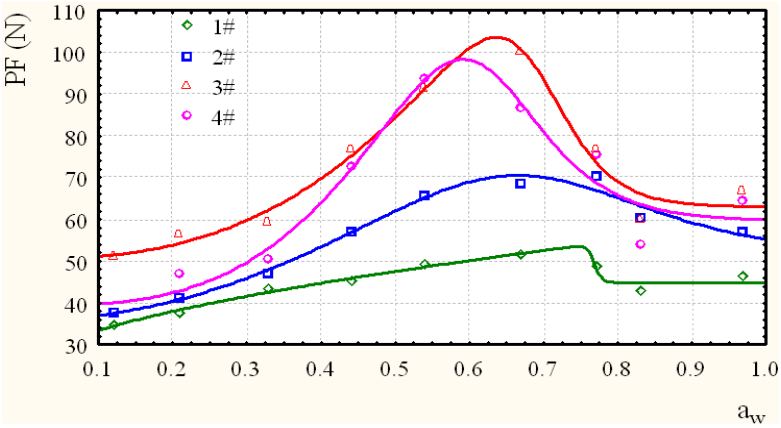

Fig. 5: PF values of the four extrudates after equilibrated at nine a_w levels (symbols) and fitting curves using MP-F model (lines)

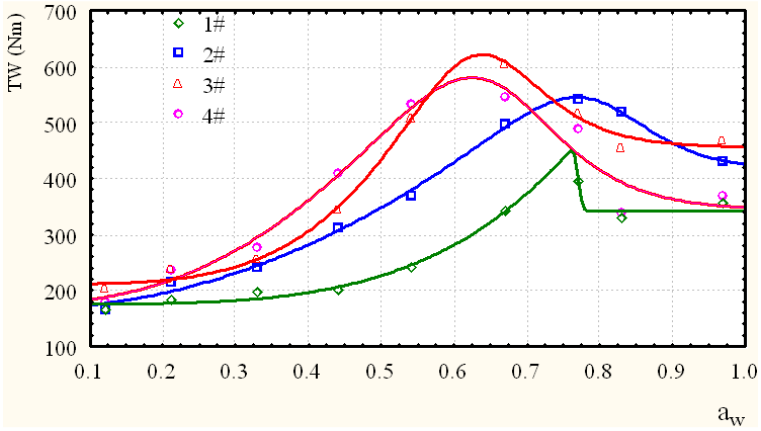

Fig. 6: TW values of the four extrudates after equilibrated at nine a_w levels (symbols) and fitting curves using MP-F model (lines)

increase cannot continue indefinitely and beyond a certain level it decreased, which indicates softening effect of hydration. When a_w reached to 0.97, both *PF* and *TW* of 1#, 3# and 4# samples appeared increase again.

As for the pattern difference among extrudate kinds, the distinct one was that the 1# sample had a convex curve in *PF*-a_w relationship before *PF* decrease. While all the other samples had a concave curve in both PF-a_w and *TW*-a_w relationship, indicating an accelerated increase. The a_w locations where the highest values of *TW* and *PF* were reached were different among the four extrudates, with 1# and 2# samples having higher a_w locations then the other two samples. There were also noticeable differences in the decrease sharpness among the four extrudates. 4# sample had a very narrow transition a_w rang in both *TW* and *PF* versus a_w curves than the other three samples.

Although the four samples were made from the same homogeneous batch of foxtail millet grain, they differed in diameter, bulk density and pore size characters. There was no significant difference in moisture content among the four extrudates (Fig. 2). The much different texture response to a_w increase among the products would attribute to their structural difference. A high-density cornmeal extrudate is more susceptible to hardening effect than is a low-density one (George *et al*., 1989). While Fig. 5 and 6 demonstrate that 3# sample, which had much lower density than 4# sample, experienced almost same magnitude of hardening effect. It can be inferred that the bulk density alone could not explain the difference found among the extrudates totally. Cell morphology has to be taken into account for mechanical properties. We hypothesize that the extrudates with fine and homogeneous structure (e.g., 4# sample) would demonstrate higher degree of hardening effect than the extrudates with coarse and heterogeneous structure (e.g., 1# sample).

Figure 6 and 7 clearly showed that the relationship between both the peak force and work of compression and water activity in the extrudate samples was curvilinear before decrease occurring and could not be approximated by the Peleg-Fermi equation. Then its modified version Eq. (5) was fitted to the experimental data. The *PF* model was also fitted for comparison. Results are presented in Table 2.

The values of S*EE* and *MRD* from MP-F model fitted to *TW* and *PF* of the four extrudates were always

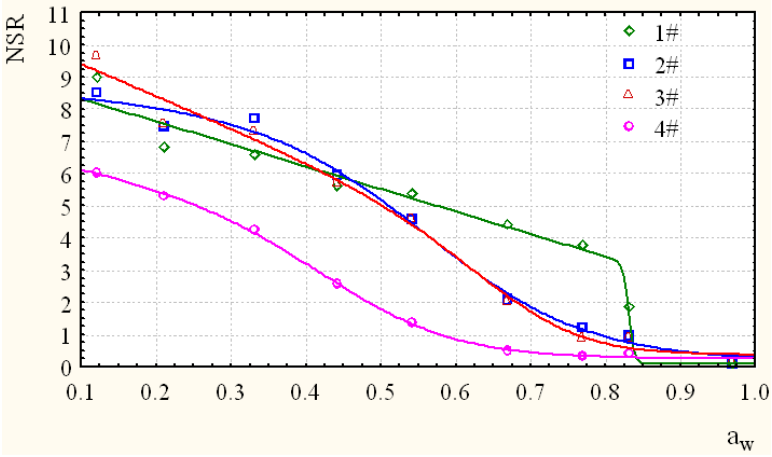

Fig. 7: NSR values of the four extrudates after equilibrated at nine a_w levels (symbols) and fitting curves using MP model (lines)

Table 2: Fitting comparison of Peleg-Fermi model (Eq. (4)) and its modified form (Eq. (5))

		TW				PF			
Sample	Model	SEE	RSS	MRD	R	SEE	RSS	MRD	R
1#	P-F	20.39	1663.65	0.1027	0.9790	1.54	9.53	0.0181	0.9460
1#	MP-F	6.07	184.47	0.0306	0.9939	1.27	8.12	0.0175	0.9839
2#	P-F	15.69	985.80	0.0654	0.9900	2.43	23.56	0.0233	0.9880
2#	MP-F	5.41	146.14	0.0245	0.9980	2.17	23.63	0.0196	0.9895
3#	P-F	26.80	2873.55	0.0942	0.9700	5.78	133.65	0.0457	0.9668
3#	MP-F	7.64	292.11	0.0279	0.9964	4.00	79.97	0.0357	0.9818
4#	P-F	20.27	1643.02	0.0601	0.9400	8.99	323.29	0.0891	0.9660
4#	MP-F	17.85	1592.54	0.0594	0.9761	6.05	183.28	0.0611	0.9770

Table 3: Regression parameters of the Peleg-Fermi Eq. (4) and its modified form Eq. (5) applied to TW and PF changes of the four extrudates caused by vapor sorption

Texture	Sample	Model	Y_0	Y_r	k	a_{wc}	b	n
TW	1#	P-F	125.48	354.85	581.39	0.80	0.0010	1.00
TW	1#	MP-F	175.80	341.87	3251.62	0.77	0.0025	4.04
TW	2#	P-F	72.75	431.63	549.58	0.83	0.0025	1.00
TW	2#	MP-F	167.15	416.03	743.52	0.81	0.0487	2.04
TW	3#	P-F	144.02	359.63	163.61	0.66	0.0053	1.00
TW	3#	MP-F	211.67	455.34	872.77	0.64	0.0466	3.88
TW	4#	P-F	64.85	459.70	759.46	0.76	0.0038	1.00
TW	4#	MP-F	176.31	343.92	1516.96	0.67	0.0584	2.30
PF	1#	P-F	31.58	44.90	31.30	0.77	0.0035	1.00
PF	1#	MP-F	24.28	44.90	34.75	0.77	0.0046	0.58
PF	2#	P-F	28.89	56.62	62.59	0.79	0.0265	1.00
PF	2#	MP-F	35.85	51.64	108.01	0.70	0.0952	1.98
PF	3#	P-F	35.72	63.31	95.32	0.77	0.0031	1.00
PF	3#	MP-F	50.59	62.98	199.48	0.69	0.0393	2.56
PF	4#	P-F	19.08	59.68	125.25	0.70	0.0433	1.00
PF	4#	MP-F	39.44	59.63	399.34	0.62	0.0532	3.04

lower than these from P-F model. As for *RSS*, except value of 1 # sample in term of *PF*, all the other *RSS* from MP-F model were lower than the values from P-F model. The *R* values from MP-F model were always higher than these from P-F model. These indicated that the M-PF model fitted the experimental data better than the P-F model.

The parameters derived from the MP-F model are presented in Table 3. All the *n* values were higher than 1 except that for the case of *PF* of 1# sample, which was in line with Fig. 5. With all the samples, the a_{wc} derived after fitting the both *PF* and *TW* data of each extrudate to the MP-F equation was lower than or equal to these from fitting using the P-F model. The a_{wc} values of both *PF* and *TW* from the MP-F model ranged from 0.62 to 0.8. These values are comparable with the results published for French bread croutons and pumpernickel (Harris and Peleg, 1996). The exact a_{wc} location of texture properties shows variations mainly with the extrudate kinds and to some extent with the properties studied. For all the four texture properties, 4# sample had the lowest a_{wc} values, while 1# sample had relative higher a_{wc} values than the other three samples.

The Y_0, *k* and *b* values derived from fitting the MP-F model were higher than the values from P-F model except the case of *PF* of 1# sample. Both models gave

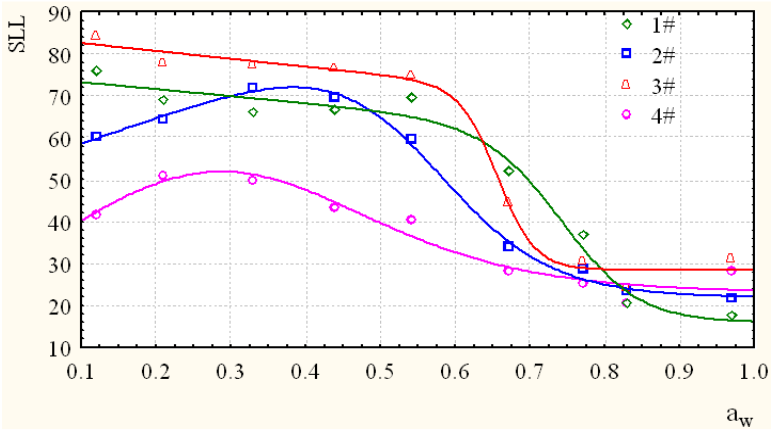

Fig. 8: SLL values of the four extrudates after equilibrated at nine a_w levels (symbols) and fitting curves using MP model (lines)

Table 4: Estimated parameters from fitted P-F model relating NSR and SLL of the four extrudates and water activity

Texture	Sample	Y_0	Y_r	k	a_{wc}	b	R
NFR	1#	9.02	0.07	-7.00	0.83	0.0038	0.988
NFR	2#	8.60	0.15	-1.59	0.57	0.1084	0.996
NFR	3#	10.40	0.37	-9.92	0.68	0.0741	0.994
NFR	4#	6.70	0.24	-4.57	0.45	0.0909	0.999
SLL	1#	74.85	15.77	-16.70	0.78	0.0518	0.993
SLL	2#	52.22	21.76	63.93	0.56	0.0748	0.997
SLL	3#	84.39	28.42	-18.77	0.66	0.0252	0.993
SLL	4#	28.28	22.92	138.25	0.42	0.1169	0.963

almost equal Y_r values. The values of *b*, describing the rate of loss of texture parameters, were between 0.0036 and 0.0584 for *TW* and between 0.0046 and 0.0952 for *PF*. These values are also comparable to data from P-F model fitting for French bread and pumpernickel (Harris and Peleg, 1996). The much lower *b* value of 1# sample reflected its rapid decrease in *PF* and *TW* as shown in Fig. 5 and 6, respectively.

Modeling NSR and SLL: Figure 7 and 8 present the *NSR* and *SLL* values of the four extrudate samples as a function of a_w. As can be seen, the *NSR* and *SLL* of 4# sample are obviously lower than these of the other three samples. As for *NSR*, there is no sensible different among 1#, 2# and 3# samples when a_w is lower than about 0.54. When a_w increased from 0.54 to 0.75, 1# sample had higher *NSR* value. For all the samples, their *NSR* reduced to a very low level when a_w reached to 0.97. This is because that at such high a_w level all the samples exhibited only on peak in their force-displacement curves. Obvious difference existed among the *SLL* values of different extrudates. This difference was lessened with a_w increase up to 0.85, but enlarged with a_w further increase to 0.97. For the 4# sample, because of its more numerous and smaller cells, the overlap of the fracture events might have contributed to the less force peak and drop-off during compression and gave much lower *NSR* and *SLL* values.

NSR decreased gradually with moisture sorption followed by a faster decrease then level off for all the four samples (Fig. 7). For the 4# sample the drop in *NSR* was considerably dramatic than the corresponding drop in the other three extrudates. As for *SLL*, its values decreased before a rapid decrease for 1# and 3# samples, while increased to a maximum before decrease for 2# and 4# samples (Fig. 8).

As shown in Fig. 7 and 8, the relation between *NSR*, *SLL* with a_w was almost linear before the onset of decrease for all the four samples. Peleg-Fermi model was used to fit the *NSR* and *SLL* data obtained at various a_w levels. The result curves were also showed in Fig. 7 and 8, respectively. Resulted model parameters are presented in Table 2. The *R* values for all cases were >0.988, indicating that the influence of water activity on both the *NSR* and *SLL* of the curves of the four foxtail millet extrudates during compression was satisfactorily described by the P-F model.

As can be seen in Table 4, the a_{wc} values of 1# were highest and these of sample 4# were lowest among the four extrudates in term of both *NSR* and *SLL*. The a_{wc} values obtained from *SFR* and *SLL* are very close to each other for the same extrudate. The values of the *k* and *b* varied considerably among the tested materials. This is a reflection of structural and compositional differences. The a_{wc} of cracker-bread determined from fitting Ferm model to force curve length was 0.51 and *b* was 0.18 (Arimi *et al*., 2010).

Modeling crispness index: The up then down course of *TW* and *PF* with a_w increase (Fig. 5 and 6) indicated that a special pair of a_w points, one higher and one lower; will give the same *TW* or *PF* value. Similar trend was also observed for *SSL* of 2# and 4# samples. This means that a_w cannot act as a effective criteria for

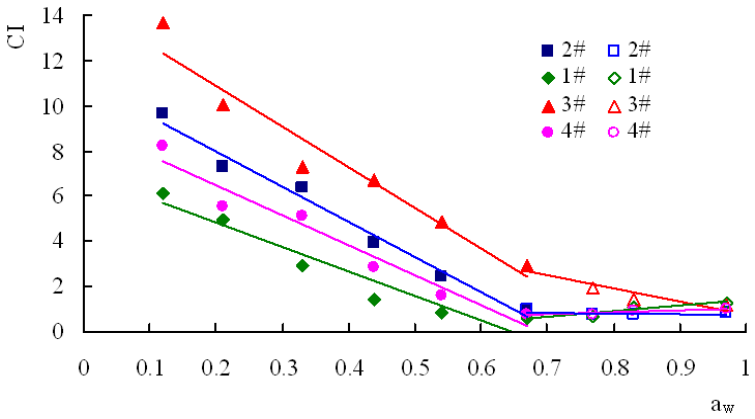

Fig. 9: Crispness index values (symbols) of the four extrudates plotted against a_w and linear fitting results in two a_w regions (lines)

predicting or controlling the texture properties of foxtail millet extrudates. Crispness index was introduced to combine the force-related and jaggedness-related measures of texture of the materials. The variation of *CI* of the four extrudates was plotted against a_w (Fig. 9). The *CI* magnitude order of the four samples was 3#>2#>4#>1#, different from the sequence based on *TW*, *PF*, *SLL* or *NSR* values, but identical the sequence based on sensory acceptability evolution conducted privately.

As can be seen from Fig. 9, a nearly linear decrease of crispness index occurred between 0 and about 0.65 (a_w), after which *CI* decreased slightly for 3# sample or kept almost constant for other three samples. The former six and later four *CI* data were correlated linearly with their corresponding a_w values for each extrudate. The linear correlation coefficients R^2 between *CI* and a_w calculated from the first six points were higher than 0.93 Eq. (10). Slopes of the fitted lines ranged from 10.76 to 18.01 depending on extrudate kinds. This difference in slope is hypothesized due to their structural variation:

$$CI = \begin{cases} 6.96 - 10.76a_w & (R^2 = 0.93) \quad 1\# \\ 11.12 - 15.61a_w & (R^2 = 0.98) \quad 2\# \\ 14.52 - 18.01a_w & (R^2 = 0.95) \quad 3\# \\ 9.16 - 13.30a_w & (R^2 = 0.95) \quad 4\# \end{cases} \qquad (10)$$

Although constant sensory intensity at lower a_w range was well documented in literatures (Sauvageot and Blond, 1991; Roudaut *et al*., 1998; Pamies *et al*., 2000; Roudaut *et al*., 2004), linear decline of sensory crispness acceptability with a_w increase from 0 to a certain a_w level was also observed for potato chip (Katz and Labuza, 1981), ice cream cone (Goerlitz *et al*., 2007) and extrudated starch (Pamies *et al*., 2000). Crispness index, calculated as the ratio of linear distance to the product of compression work and mean force, can discriminate the sensory crispness of extrudated rice after equilibrium with different a_w levels (Heidenreich *et al*., 2004). These findings suggested that the combined criteria of force-related and jadggnes-related parameters from force-displacement, such as *CI* defined in this article, might be a good crispness measure of cellular extrudate products at low-intermediate a_w range.

The critical water activity for *CI* complete loss was obtained from the intersection between the two straight lines for each extrudate. The resulting values for 1#, 2#, 3# and 4 # samples was a_w 0.66, 0.61, 0.65 and 0.64, respectively, which seem not dependent on the product kind. The similarity is probably a result of similar chemical composition. The critical a_w or water constant level beyond which sensory crispness is lost almost completely is about 0.6 for extrudated waxy corn starch (Pamies *et al*., 2000), 0.74 for a crispy snack model (Roos *et al*., 1998), 11% for extrudated bread (Roudaut *et al*., 1998), 14% for rice krispy (Sauvageot and Blond, 1991).

Previous reports indicated that BET monolayer moisture content was a good indicator of the initial loss of crispness for saltine crackers, popcorn, puffed corn curls, potato chips and puffed rice cakes (Katz and Labuza, 1981) and corn cake (Li *et al*., 1998), while not a useful critical parameter for the change in crispness of the tapioca-flour-based baked products (Kulchan *et al*., 2010). The monolayer moisture content in this work was 6.21% beyond which no noticeable rapid increase or decrease in force- or curve jaggedness-related texture parameters was observed. This suggested that monolayer moisture content cannot act as an indicator of mechanical texture changes for foxtail millet extrudates.

CONCLUSION

Moisture sorption resulted jaggedness loss of the force-displacement curves, indicating fracture mechanics transaction from brittle to plastic fracture and finally to elastic deformation. Moisture sorption

affected different mechanical textures of foxtail millet extudates in different ways with respect to texture increase or decrease before a rapid decrease, a_w location and range where a rapid decrease occurring and the speed of the decrease and increase with aw. The a_{wc} values depended mainly on the kinds of the extrudates and to some extent on the texture properties studied. The extrudate with coarse structure exhibited lower force-related texture parameters, while the extrudate with fine structure exhibited lower jaggedness-related texture values.

The relation between both *NSF*, *SSL* and a_w can be well described by the Peleg-Fermi model. While the relation between both *TW*, *PF* and a_w can be described better by the modified Peleg-Fermi model proposed here. Crispness index decreased almost linearly as a_w increase up to 0.61-0.66 which appeared independent of extrudate kind.

ACKNOWLEDGMENT

We wish to thank the financial support for this work from the National Project of Transformation of Scientific and Technological Achievements of China (05EFN216900373).

REFERENCES

Arimi, J.M., E. Duggan, M. O'Sullivan, J.G. Lyng and E.D. O'Riordan, 2010. Effect of water activity on the crispiness of a biscuit (Crackerbread): Mechanical and acoustic evaluation. Food Res. Int., 43: 1650-1655.

Barret, A.H. and G. Kaletunc, 1998. Quantitative description of fracturability changes in puffed corn extrudates affected by sorption of low levels of moisture. Cereal Chem., 75(5): 695-698.

Braga, L.L.M. and R.L. Cunhn, 2004. Plasticization and antiplasticization of small molecule in cellular foods: TMDSC and mechhanical properties. Int. J. Food Prop., 7(1): 105-120.

Chang, Y.P., P.B. Cheah and C.C. Seow, 2000. Variations in flexural and compressive fracture behavior of a brittle cellular food (dried bread) in response to moisture sorption. J. Texture Stud., 31: 525-540.

Chauvin, M.A., F. Younce, C. Ross and B. Swanson, 2008. Standard scales for crispness, crackliness and crunchiness in dry and wet foods: Relationship with acoustical determinations. J. Texture Stud., 39: 345-368.

Colonna, P., J.L. Doublier, J.P. Melcion, F. de Monredon and C. Mercier, 1984. Extrusion cooking and drum drying of wheat starch. I. Physical and macromolecular modifications. Cereal Chem., 61(6): 538-541.

George, W., S.W. Halek and K.L.B. Chang, 1989. The effect of moisture content on mechanical properties and texture profile parameters of corn meal extrudates. J. Texture Stud., 20: 43-55.

Gibson, L.J. and M.F. Ashby, 1999. Cellular Solids: Structure and Properties. 2nd Edn., Pergamon Press, Oxford, U.K.

Goerlitz, C.D., W.J. Harper and J.F. Delwiche, 2007. Relationship of water activity to cone crispness as assessed by positional relative rating. J. Sens. Stud., 22: 687-694.

Gondek, E. and P.P. Lewicki, 2006. Antiplasticization of cereal-based products by water. Part II: Breakfast cereals. J. Food Eng., 77: 644-652.

Greenspan, L., 1977. Humidity fixed points of binary saturated aqueous solutions. J. Res. Natl. Bur. Stand., 81: 89-96.

Guo, X.E. and L.J. Gibson, 1999. Behavior of intact and damaged honeycombs: A finite element study. Int. J. Mech. Sci., 41: 85-105.

Harris, M. and M. Peleg, 1996. Patterns of textural changes in brittle cellular cereal foods caused by moisture sorption. Cereal Chem., 73(2): 225-231.

Heidenreich, S., D. Jaros, H. Rohm and A. Ziems, 2004. Relationship between water activity and crispness of extruded rice crisps. J. Texture Stud., 35: 621-633.

Katz, E.E. and T.P. Labuza, 1981. Effect of water activity on the sensory crispness and mechanical deformation of snack food products. J. Food Sci., 46: 403-409.

Kulchan, R., P. Suppakul and W. Boonsupthip, 2010. 54 Texture of Glassy Tapioca-flour-based Baked Product as a Function of Moisture Content. In: Reid, D.S., T. Sajjaanantakul, P.J. Lillford and S. Charoenrein (Eds.), Water Properties in Food, Health, Pharmaceutical and Biological Systems: ISOPOW 10. Wiley-Blackwell, Ames, Iowa, pp: 591-598.

Lane, R.H., 1998. Cereal Foods. In: Official Methods Analysis of the Association of Official Analytical Chemists. 16th Edn., AOAC International, Gaithersburg, MD, pp: 1-37.

Lewicki, P., E. Jakubczyk, A. Marzec, M.C. Cabral and P.M. Pereira, 2004. Effect of water activity on mechanical properties of dry cereal products. Acta Agrophysica, 4(2): 381-391.

Li, Y., K.M. Kloeppel and F. Hsieh, 1998. Texture of glassy corn cakes as a function of moisture content. J. Food Sci., 63(5): 1-4.

Martinez-Navarrete, N., G. Moraga, P, Talens and A. Chiralt, 2004. Water sorption and the plasticization effect in wafers. Int. J. Food Sci. Tech., 39: 555-562.

Marzec, A. and P.P. Lewicki, 2006. Antiplasticization of cereal-based products by water. Part I. Extruded flat bread. J. Food Eng., 73(1): 1-8.

Nicholls, R.J., I.A.M. Appelqvist, A.P. Davies, S.J. Ingman and P.L. Lillford, 1995. Glass transition and fracture behaviour of gluten and starches within the glassy state. J. Cereal Sci., 21(1): 25-36.

Norton, C.R.T., J.R. Mitchell and J.M.V. Blanshard, 1998. Fractal determination of crispy or crackly textures. J. Texture Stud., 29: 239-253.

Pamies, V.B., G. Roudaut, C. Dacremont, L. Meste and J.R. Mitchell, 2000. Understanding the texture of low moisture cereal products: Mechanical and sensory measurements of crispness. J. Sci. Food Agr., 80: 1679-1685.

Roos, Y.H., K. Roininen, K. Jouppila and H. Tuorila, 1998. Glass transition and water plasticization effects on crispness of a snack food extrudate. Int. J. Food Prop., 1(2): 163-180.

Roudaut, G. and D. Champion, 2011. Low-moisture food: A physicochemical approach to investigate the origin of their physical instability versus water or sucrose. Food Biophys., 6: 313-320.

Roudaut, G., C. Dacremont and M.L. Meste, 1998. Influence of water on the crispness of cereal-based foods: Acoustic, mechanical and sensory studies. J. Texture Stud., 29: 199-213.

Roudaut, G., F. Poirier, D. Simatos and M.L. Meste, 2004. Can dynamical mechanical measurements predict brittle fracture behaviour? Rheol. Acta, 44: 104-111.

Saeleaw, M., K. Dürrschmid and G. Schleining, 2012. The effect of extrusion conditions on mechanical-sound and sensory evaluation of rye expanded snack. J. Food Eng., 110: 532-540.

Sauvageot, F. and G. Blond, 1991. Effect of water activity on crispness of breakfast cereals. J. Texture Stud., 22: 423-442.

Surówka, K., 2002. Food texture and methods of its study (In Polish). Przemysł SpoŜywczy, 10: 12-17.

Suwonsichon, T. and M. Peleg, 1998. Instrumental and sensory detection of simultaneous brittleness loss and moisture toughening in three puffed cereals. J. Texture Stud., 29: 255-274.

Wollny, M. and M. Peleg, 1994. A model of moisture-induced plasticization of crunchy snacks based on Fermi's distribution function. J. Sci. Food Agr., 64: 467-473.

Zhao, X.W., 2006. Extrusion characteristics of foxtail millet. Ph.D. Thesis, Northwest Science and Technology University for Agricultural Forestry, Yangling, Shaanxi.